Probing Hot Electron Flow Generated on Pt Nanoparticles with Au/TiO_2 Schottky Diodes during Catalytic CO Oxidation

Jeong Y. Park[1], Hyunjoo Lee[1], J. Russell Renzas[1], Yawen Zhang[1,2], and

Gabor A. Somorjai[1,]*

[1]Department of Chemistry, University of California, Berkeley, CA 94720
Materials Sciences Division and Chemical Sciences Division, Lawrence Berkeley National Laboratory, Berkeley, CA 94720
[2]College of Chemistry and Molecular Engineering, and the State Key Lab of Rare Earth Materials Chemistry and Applications & PKU-HKU Joint Lab in Rare Earth Materials and Bioinorganic Chemistry, Peking University, Beijing 100871, China

Abstract

Hot electron flow generated on colloid platinum nanoparticles during exothermic catalytic carbon monoxide oxidation was directly detected with Au/TiO_2 diodes. Although Au/TiO_2 diodes are not catalytically active, platinum nanoparticles on Au/TiO_2 exhibit both chemicurrent and catalytic turnover rate. Hot electrons are generated on the surface of the metal nanoparticles and go over the Schottky energy barrier between Au and TiO_2. The continuous Au layer ensures that the metal nanoparticles are electrically connected to the device. The overall thickness of the metal assembly (nanoparticles and Au thin film) is comparable to the mean free path of hot electrons, resulting inballistic transport through the metal. The chemicurrent and chemical reactivity of nanoparticles with citrate, hexadecylamine, hexadecylthiol, and TTAB (Tetradecyltrimethylammonium Bromide) capping agents were measured during catalytic CO oxidation at pressures of 100 Torr O_2 and 40 Torr CO at 373~513 K. We found that chemicurrent yield varies with each capping agent, but always decreases with increasing temperature. We suggest that this inverse temperature dependence is associated with the influence of charging effects due to the organic capping layer during hot electron transport through the metal-oxide interface.

*****To whom correspondence should be addressed. E-mail:somorjai@berkeley.edu

Most heterogeneous catalysts are highly dispersed metal nanoparticles supported on porous oxides[1-4]. The phenomena associated with reduced size, such as the variation of reaction intermediates with metal nanoparticle size and shape and the role of the oxide-metal interface, are fundamental questions in catalysis. Synthesis of nanoparticles by colloid chemistry has been one of major directions to address these questions [5]. Monodisperse platinum and rhodium nanoclusters are synthesized in solution and capped with an organic or polymer film to prevent their aggregation[4, 6]. Two dimensional nanoparticle systems have been synthesized by depositing nanoparticles on an oxide support using the Langmuir-Blodgett technique, which controls packing density. The size (1-12 nm), composition, and shape of nanoparticles are found to be important factors influencing reaction activity and selectivity[4, 7 , 8, 9].

Atomic or molecular processes in metals can generate hot electrons with kinetic energies of 1-3 eV and mean free paths in the range of 5-10 nm [10, 11]. If the metal thickness is of the order of the electron mean free path, hot electrons can be collected during ballistic transport across the metal. Recent experimental [11-14] and theoretical [10, 15] studies have demonstrated electronic excitations created during chemisorption and physisorption of gases at surfaces, and by chemical reactions at surfaces [16-18].

The oxide-metal interface is one of the major factors which determines the activity and selectivity of the heterogeneous catalysts[19-21]. It was observed that during certain reactions the oxide onto which the metal nanoparticles are deposited can dramatically change activity and selectivity even though the oxide itself is not active in catalysis[22, 23]. Earlier studies by Schwab [24] suggest that a Schottky barrier is formed at the oxide-metal interface and charge transport through the interface could be responsible for the enhanced catalytic reactivity. In order to elucidate these phenomena, it is important to measure hot electron transport between the nanoparticles and oxide.

In this article, we present a novel scheme for the detection of hot electrons generated on colloid nanoparticles under catalytic reaction conditions using Au/TiO_2 diodes. The nanoparticle-nanodiode hybrid system is composed of platinum nanoparticles, Au thin film (2.5 nm thick), TiO_2, and Ti/Au Ohmic contacts. The energy diagram and schematic of the nanoparticle-nanodiode hybrid system are shown in Figures 1a and 1b, respectively. The interface between Au and TiO_2 forms a Schottky barrier with an energy barrier of about 1.0 eV. Hot electrons are generated on the surface of the platinum metal nanoparticles during the exothermic catalytic reaction of CO oxidation, and go over the energy barrier between Au and TiO_2. The overall thickness of the metal assembly (nanoparticles and Au thin film) is comparable to the electron mean free path, resulting in the ballistic transport of hot electrons through the metal.

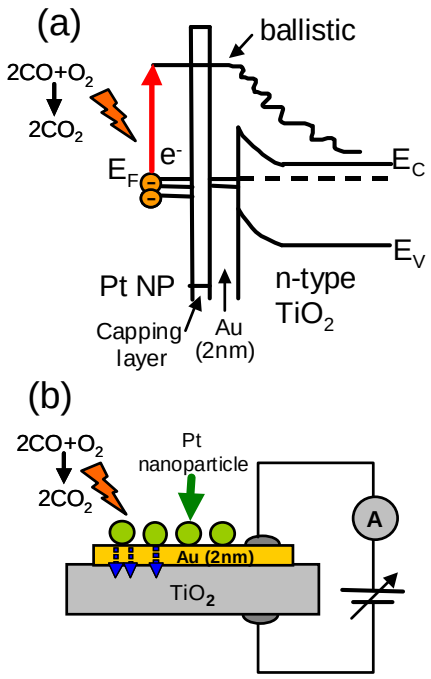

Figure 1. (a) Energy diagram and (b) schematic of hot electron generation in nanoparticles on Au/TiO_2 Schottky diode. Schottky barrier is the energy barrier between the metal and the semiconductor. The hot electrons overcome the Schottky barrier and turn into low-energy electrons in the semiconductor when the excess energy is larger than the Schottky barrier height.

Platinum colloid nanoparticles with four types of capping layer have been used; TTAB (Tetradecyltrimethylammonium Bromide), hexadecylamine (HDA), hexadecylthiol (HDT), and citrate. Figures 2a and 2b show TEM images of TTAB and citrate coated Pt nanoparticles. TTAB (Tetradecyltrimethylammonium Bromide) capped nanoparticles were synthesized as previously reported[25]. Briefly, 1mM aqueous K_2PtCl_4 in 100 mM TTAB was reduced by 30 mM $NaBH_4$ at 50^{o}C. Excess H_2 evolved from the reacting solution was released by inserting a needle into the septum. After 7 hours, the

reaction was allowed to cool to room temperature and left overnight to decompose the remaining $NaBH_4$ in water. The Pt nanoparticles were collected and washed by repeated centrifugation and sonication. TTAB stabilized Pt nanoparticles have the shape of cubes and an average size of 12.3 (±1.4) nm. Organic capping layer was exchanged with hexadecylamine (HDA) or hexadecylthiol (HDT). 8ml of TTAB capped nanoparticles were redispersed in 2 ml of deionized water after washing, then 10 mg of HDA or 20 µl of HDT was added to the washed nanoparticles. The solution was refluxed overnight at 50^{o}C. Then, the residual HDA or HDT was washed with ethanol. The nanoparticles were further washed by dispersing in chloroform and precipitating with hexane. Finally, the nanoparticles were dispersed in chloroform and deposited on a diode. HDA and HDT capped nanoparticles had an average size of 12.3 (±1.4) nm with cubic shapes.

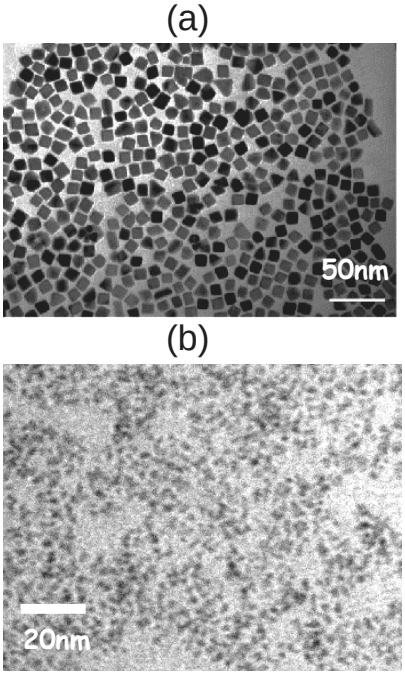

Figure 2. (a) TEM images of TTAB coated Pt nanoparticles and (b) citrate capped Pt nanoparticles.

Citrate-stabilized Pt nanoparticles were also prepared as previously reported[26]. 20ml of 1mM K_2PtCl_4 solution was refluxed while stirring for 1 hour at 110^{o}C, followed by the quick addition of 2ml of 38.8 mM trisodium citrate solution. The mixture was stirred for 1 hour additionally. After cooling the solution, the nanoparticle solution was centrifuged at 14000 rpm for 30 min, followed by the dispersion of the precipitates in DI water. The citrate-stabilized Pt nanoparticles were 3.6 ± 0.5 nm in size, based on TEM images.

Nanoparticles were deposited on Au/TiO_2 diodes using both drop-casting and the Langmuir-Blodgett (LB) technique [9]. The procedures for nanoparticle deposition using LB techniques are described in Figure S1a of the supplemental materials. An SEM image

of a nanoparticle array on the diode surface is shown in Figure S1b. The number of metal sites is calculated using geometrical considerations based on scanning electron microscopy (SEM) measurements of the surface area of a nanoparticle array.

Details on the fabrication of the Schottky diodes are described elsewhere [17, 27]. Vertically-oriented Au/TiO_2 Schottky diodes were fabricated on an insulating p-type Si(100) wafer covered with 100 nm of thermally grown SiO_2. Reactive direct current (DC) magnetron sputtering was used to deposit approximately 150 nm titanium oxide through an aluminum shadow mask. During sputtering, bias voltage was 430 V, O_2 pressure was 11-12 sccm, and Ar pressure was 37 sccm. The film was then annealed in air at 600 °C for one hour to promote crystallization and full integration of oxygen into the oxide lattice. Next, ohmic contacts composed of 30 nm Ti and 100 nm Au were deposited onto both the TiO_2 and the insulating SiO_2. The contact on the TiO_2 provided an ohmic back contact and the contact on the SiO_2 was made to facilitate electrical connection to the thin Au Schottky contact. A 10 nm Au film was then deposited between the SiO_2 contact pad and over the edge of the bare TiO_2. This layer was thick enough to provide continuous electrical contact over the step edge of the TiO_2. Finally, a 2 nm Au pad was deposited partially on top of the 10 nm Au layer and partially on top of the bare TiO_2. The area of the 2 nm Au layer directly contacting the TiO_2 was ~ 1 mm^2. All metals were deposited using electron beam evaporation through aluminum shadow masks. Thicknesses were monitored during evaporation using a standard quartz crystal monitor. We verified that the 2 nm Au layer forms a continuous film using atomic force microscopy measurements. The rms (root mean square) roughness of this film is 0.4 nm.

The formation of a Schottky barrier between Au and TiO_2 has been previously reported. Tang et al. fabricated an Au/TiO_2 diode and obtained a Schottky barrier height of 0.9 eV based on thermionic emission theory[28]. This energy barrier is high enough to suppress the contribution of electron flow from the thermal excitation of electrons. In order to determine barrier heights and ideality factors for the nanodiodes, we fit the I-V curves of our devices to the thermionic emission equation. For thermionic emission over the barrier, the current density of Schottky contacts as a function of applied voltage is

given by [29]

$$I = FA^{*}T^{2}\exp\left(-\frac{\Phi_n}{k_B T}\right)\cdot\left[\exp\left(\frac{e_0\left(V_a - R_S I\right)}{\eta k_B T}\right) - 1\right] \qquad (1)$$

where F = Area, A^{*} = Effective Richardson Constant, Φ_n = Schottky Barrier Height, η = Ideality Factor, and R_s = Series Resistance, respectively. Figure 3 shows the current-voltage plots of an Au/TiO_2 diode before and after deposition of TTAB capped nanoparticles, indicating that the rectifying character of the diode remains the same. The Schottky barrier height of the diode, as obtained using the thermionic emission model [29], was 1.0 eV prior to nanoparticles deposition and 0.96 eV after, indicating that nanoparticle deposition does not significantly affect the electrical properties of the system. The ideality factor increases slightly from 2.2 to 2.3 after deposition of nanoparticles.

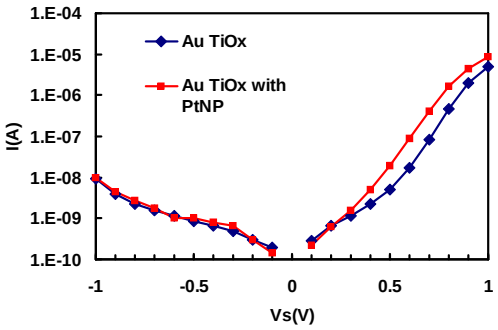

Figure 3. I-V curves of Au/TiO_2 diode before and after deposition of TTAB capped nanoparticles.

A batch reaction system combined with electrical measurement capability was built to carry out the gas phase reaction. The design of the reaction cell has been described elsewhere [17]. The reaction cell was evacuated down to 5 x 10^{-8} Torr by a turbo molecular pump. A ceramic heater was used to change the temperature at the sample and a Type-K thermocouple was used to measure temperature at the sample surface. The temperature controller provided feedback to the current applied to the heater which kept the fluctuations of the temperature below 0.5 ^{o}C. A sampling loop, including a gas chromatograph and a circulation pump, continuously measured reaction rates from reactant and product concentrations.

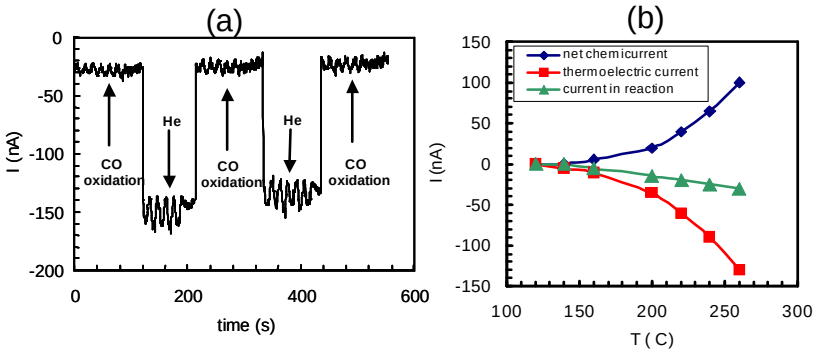

Figure 4. (a) Current measured under He (thermoelectric current) and measured in reaction conditions on citrate capped platinum nanoparticles on Au/TiO_2 diode. (b) The difference between the thermoelectric current and reaction current is associated with the net chemicurrent.

The current signal from the device was measured using a Keithley 2400 Sourcemeter at 0 V bias. Gold wires made contact to the two contact pads of the device and current generated across the Au/TiO_2 Schottky barrier by the citrate capped Pt nanoparticles was measured both under reaction conditions and under pure He, as shown in Figure 4a. When the diode is in 1 atmosphere He, only the thermoelectric current due to the elevated temperature is observed. This thermoelectric current is caused by the difference in electrical potential between two electrodes because of the Seebeck effect. The high thermoelectric current of the TiO_2-based diode is associated with the high Seebeck coefficient of TiO_2, which is 0.6 mV/K [30]. Figure 4b shows the thermoelectric current and chemicurrent measured on the nanoparticle/diode system. The difference in the currents between the thermoelectric current (under He condition) and reaction condition (in the mixture of reactant gases, O_2 (100Torr) and CO (40 Torr), and He (620 Torr)) is attributed to the hot electron chemicurrent generated by the CO oxidation reaction taking place at the nanoparticle surfaces. In contrast, Au/TiO_2 diodes showed no turnover rate or chemicurrent (up to 280 ^{o}C) within our detection range, as shown in the supporting information, which suggests that Au/TiO_2 diodes are not catalytically active.

Figure 5 shows the plot of turnover rate, chemicurrent, and chemicurrent yield measured on citrate capped Pt nanoparticles on the Au/TiO_2 diode as a function of temperature. Interestingly, the activation energy estimated with the measurement of turnover rate is 28 kcal/mol, significantly higher than that of chemicurrent (14 kcal/mol).

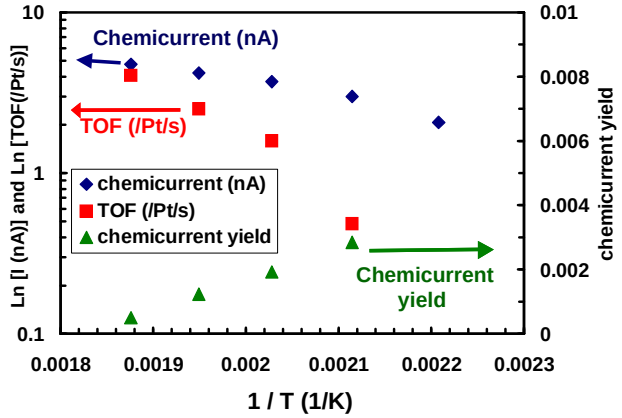

Figure 5. (a) The plot of turnover rate, chemicurrent, and chemicurrent yield as a function of temperature measured on citrate capped Pt nanoparticles on Au/TiO_2 diode. The chemicurrent yield decreases with increasing temperature, which suggests that charging effects repel the flow of hot electrons.

This big difference in activation energy is in contrast to results obtained using thin film Pt/GaN and Pt/TiO_2 diodes, which exhibited the same activation energy (20-22 kcal/mol) between the chemicurrent and turnover rate measurements [27].

The difference in activation energy is attributed to a charging effect occurring at the insulating capping agent

Capping agent	Citrate	CTAB	Hexadecylthiol	Hexadecylamine
Turnover rate at 240 ^{o}C (/Pt site/s)	12.4 ± 2.3	5.3 ± 1.0	3.4 ± 0.6	3.2 ± 0.4
Activation energy from turnover rate (kcal/mol)	27.3 ± 0.9	28.0 ± 1.2	27.6 ± 1.4	27.5 ± 1.0
Chemicurrent at 240 ^{o}C (nA)	65 ± 6	20 ± 4	6 ± 2	5 ± 2
Activation energy from chemicurrent (kcal/mol)	14.2 ± 1.5	15.4 ± 2.1	16.0 ± 3.5	15.5 ± 4.7
Chemicurrent yield at 240 ^{o}C (x 10 $^{-4}$)	12.2 ± 3.4	8.7 ± 3.3	3.9 ± 2.0	3.5 ± 1.8

Table 1. Turnover rate, chemicurrent measured at 240 ^{o}C for nanoparticles with various capping layers on Au/TiO_2 diode. The chemicurrent yield is the number of hot electrons per product CO_2 molecules.

layers present at the metal-oxide interface. As the hot electrons pass through the metal oxide interface, some charges can be trapped in the insulating capping layer. These trapped charges can repel the flow of other charges, reducing the total chemicurrent. This

effect will be more prominent in the high current regime. As a result, the increase of chemicurrent with increasing temperature is slower than of the increase in turnover rate. This causes a temperature-dependent decrease in the number of hot electrons collected per CO_2 molecule produced, or chemicurrent yield.

Another possible mechanism to explain the inverse temperature dependence of chemicurrent is a Coulomb blockade induced by the hot electrons reflected back from the capping layer and equilibrated inside the nanoparticles. In this scheme, the capping layer is a barrier which electrically isolates the nanoparticles.

Table 1 shows the turnover rate and chemicurrent measured at 240^{o}C for nanoparticles with various capping layers on Au/TiO_2 diodes. Both turnover rate and chemicurrent were highest for the citrate-capped nanoparticles. This is most likely both because the citrate is composed of only five carbon chains, which implies that reactant and product molecules can travel through the short capping layer relatively efficiently. TTAB shows intermediate activity. This is attributed to the weak bonding between TTAB and the Pt atoms in the nanoparticles, which allows the reactant and product molecules to pass through the capping layer. Hexadeclyamine and hexadeclythiol, however, showed weak activity. This is because they form strong NH_2 and sulfur bonds, respectively, with Pt, which can block the reaction sites and thus lower the reaction activity. Sulfur, in particular, is well known to poison the catalytic activity of platinum surfaces during CO oxidation. [31 32]

The chemicurrent yield of nanoparticles on Au/TiO_2 systems ranges from 3-12 x 10^{-4} electrons/CO_2, which is similar to the chemicurrent yield in thin-film Pt/TiO_2 and Pt/GaN diodes of 10^{-3}-10^{-4} electrons/CO_2[18]. This similarity is attributed to the comparable overall metal thicknesses of the three systems, because the travel distance of the hot electrons in the $NP/Au/TiO_2$ diode system (sum of the size of nanoparticle and thickness of Au layers) is comparable to the thickness of the Pt thin film (5 nm) in the Pt/GaN and Pt/TiO_2 systems. The highest chemicurrent yield was observed for citrate stabilized Pt nanoparticles. This is partly due to the smaller size (3.5 nm) of citrate stabilized nanoparticles, which results in a shorter travel length for the hot electrons and more efficient hot electron transport.

We also investigated possible morphological changes in the Pt nanoparticles on the Au/TiO_2 diodes after CO oxidation up to 260 °C with SEM. As shown in Figure S3a of the supplemental materials, after the reaction we did not observe any significant change in the morphology of the nanoparticles within the resolution of SEM (~1 nm), which indicates that nanoparticle agglomeration was not a factor in our measurements. The electrical character of the nanoparticle-diode system was also checked with I-V measurement before and after the reaction. Figure S3b in the supplemental materials shows the I-V plots measured on citrate capped Pt NP on a Au/TiO_2 diode, revealing that there is no significant change in the rectifying behavior of the devices after CO oxidation. I-V curve fitting indicates that the barrier height after the reaction is 0.95 eV, which is very similar to the diode before reaction. This measurement indicates that an efficient Schottky barrier was maintained during the chemical reaction. The overall conductance of the devices increased by a factor of 5-10 during the reaction. This increased conductance can be associated with the additional contribution to electrical transport from the partial decomposition of capping layers during CO oxidation [9] as well as with possible changes in the Au/TiO_2 Schottky interface associated with prolonged heating.

Due to the significant role of the capping layers in hot electron transport, it would be of great interest to study the effect of capping layer modification and removal on chemicurrent yield. We are currently using ultraviolet exposure and oxygen plasmas to prepare exposed nanoparticles on Au/TiO_2 Schottky diodes in order to study these effects.

In conclusion, we found that Pt nanoparticles on Au/TiO_2 Schottky diodes generate hot electron current and catalytic turnover and that Au/TiO_2 alone is not catalytically active. Using nanoparticles with several different types of capping layers, we studied the influence of the capping layer on the catalytic activity and chemicurrent generation. This hybrid system of nanoparticles on a Schottky diode provides us with a novel scheme for chemical sensing using metallic nanocatalysts.

Acknowledgement

This work was supported by the Director, Office of Science, Office of Basic Energy Sciences, Division of Materials Sciences and Engineering of the U.S. Department of Energy under Contract No. DE-AC02-05CH11231. Y. W. Zhang gratefully acknowledges the financial aid of Huaxin Distinguished Scholar Award from Peking University Education Foundation of China. We thank Sergey Maximoff for his helpful comments.

References

1. Rolison, D. R. *Science* 2003, 299, (5613), 1698-1701.
2. Bell, A. T. *Science* 2003, 299, (5613), 1688-1691.
3. Somorjai, G. A.; Park, J. Y. *Physics Today* 2007, 60, 48-53.
4. Song, H.; Rioux, R. M.; Hoefelmeyer, J. D.; Komor, R.; Niesz, K.; Grass, M.; Yang, P. D.; Somorjai, G. A. *Journal of the American Chemical Society* 2006, 128, (9), 3027-3037.
5. Somorjai, G. A.; Tao, F.; Park, J. Y. *Topics in Catalysis* 2008, 47, 1-14.
6. Zhang, Y.; Grass, M. E.; Habas, S. E.; Tao, F.; Zhang, T.; Yang, P.; Somorjai, G. A. *Journal of Physical Chemistry C* 2007, 111, 12243-12253.
7. Bratlie, K. M.; Lee, H.; Komvopoulos, K.; Yang, P.; Somorjai, G. A. *Nano Letters* 2007, 7, 3097-3101.
8. Narayanan, R.; El-Sayed, M. A. *Nano Letters* 2004, 4, (7), 1343-1348.
9. Park, J. Y.; Zhang, Y.; Grass, M.; Zhang, T.; Somorjai, G. A. *Nano Letters* 2008, 8, 673 -677.
10. Gadzuk, J. W. *Journal of Physical Chemistry B* 2002, 106, (33), 8265-8270.
11. Nienhaus, H. *Surface Science Reports* 2002, 45, (1-2), 3-78.
12. Huang, Y. H.; Rettner, C. T.; Auerbach, D. J.; Wodtke, A. M. *Science* 2000, 290, (5489), 111-114.
13. Hellberg, L.; Stromquist, J.; Kasemo, B.; Lundqvist, B. I. *Physical Review Letters* 1995, 74, (23), 4742-4745.
14. Nienhaus, H.; Bergh, H. S.; Gergen, B.; Majumdar, A.; Weinberg, W. H.; McFarland, E. W. *Physical Review Letters* 1999, 82, (2), 446-449.
15. Mizielinski, M. S.; Bird, D. M.; Persson, M.; Holloway, S. *Journal of Chemical Physics* 2005, 122, (8), 084710.
16. Ji, X. Z.; Zuppero, A.; Gidwani, J. M.; Somorjai, G. A. *Journal of the American Chemical Society* 2005, 127, (16), 5792-5793.
17. Park, J. Y.; Somorjai, G. A. *Journal of Vacuum Science & Technology B* 2006, 24, (4), 1967-1971.
18. Park, J. Y.; Renzas, J. R.; Hsu, B. B.; Somorjai, G. A. *Journal of Physical Chemistry C* 2007, 111, (42), 15331-15336.
19. Boffa, A.; Lin, C.; Bell, A. T.; Somorjai, G. A. *Journal of Catalysis* 1994, 149, (1), 149-158.
20. Hayek, K.; Fuchs, M.; Klotzer, B.; Reichl, W.; Rupprechter, G. *Topics in Catalysis* 2000, 13, (1-2), 55-66.
21. Park, J. Y.; Renzas, J. R.; Contreras, A. M.; Somorjai, G. A. *Topics in Catalysis* 2007, 46, 217.
22. Tauster, S. J.; Fung, S. C.; Garten, R. L. *Journal of the American Chemical Society* 1978, 100, (1), 170-175.
23. Haller, G. L.; Resasco, D. E. *Advances in Catalysis* 1989, 36, 173-235.
24. Schwab, G. M. *Angewandte Chemie-International Edition* 1967, 6, (4), 375-&.
25. Lee, H.; Habas, S. E.; Kweskin, S.; Butcher, D.; Somorjai, G. A.; Yang, P. D. *Angewandte Chemie-International Edition* 2006, 45, (46), 7824-7828.
26. Yang, J.; Lee, J. Y.; Chen, L. X.; Too, H. P. *Journal of Physical Chemistry B* 2005, 109, (12), 5468-5472.

27. Park, J. Y.; Somorjai, G. A. *Chemphyschem* 2006, 7, (7), 1409-1413.
28. Tang, J.; White, M.; Stucky, G. D.; McFarland, E. W. *Electrochemistry Communications* 2003, 5, (6), 497-501.
29. *Using Richardson constant for TiO_2, A = 24 A/cm^2 K^2.*
30. He, Q. Y.; Hao, Q.; Chen, G.; Poudel, B.; Wang, X. W.; Wang, D. Z.; Ren, Z. F. *Applied Physics Letters* 2007, 91, (5).
31. Bonzel, H. P.; Ku, R. *Journal of Chemical Physics* 1973, 59, (4), 1641-1651.
32. Bartholomew, C. H.; Agrawal, P. K.; Katzer, J. R. *Advances in Catalysis* 1982, 31, 135-242.